

Momentum imaging spectrometer for molecular fragmentation dynamics induced by pulsed electron beam

EnLiang Wang, Xu Shan, YuFeng Shi, YaGuo Tang, and XiangJun Chen

Citation: [Review of Scientific Instruments](#) **84**, 123110 (2013); doi: 10.1063/1.4847156

View online: <http://dx.doi.org/10.1063/1.4847156>

View Table of Contents: <http://scitation.aip.org/content/aip/journal/rsi/84/12?ver=pdfcov>

Published by the [AIP Publishing](#)

Articles you may be interested in

[A combined electron-ion spectrometer for studying complete kinematics of molecular dissociation upon shell selective ionization](#)

Rev. Sci. Instrum. **84**, 073101 (2013); 10.1063/1.4811796

[Momentum-imaging apparatus for the study of dissociative electron attachment dynamics](#)

Rev. Sci. Instrum. **84**, 033104 (2013); 10.1063/1.4794093

[Positive/negative ion velocity mapping apparatus for electron-molecule reactions](#)

Rev. Sci. Instrum. **83**, 013108 (2012); 10.1063/1.3678328

[Fragmentation dynamics of argon clusters \(\$\text{Ar}_n\$, \$n = 2\$ to 11\) following electron-impact ionization: Modeling and comparison with experiment](#)

J. Chem. Phys. **124**, 184314 (2006); 10.1063/1.2194552


[Electron impact dissociative ionization of \$\text{CO}_2\$: Measurements with a focusing time-of-flight mass spectrometer](#)

J. Chem. Phys. **108**, 927 (1998); 10.1063/1.475456

JANIS

Does your research require low temperatures? Contact Janis today.

Our engineers will assist you in choosing the best system for your application.



10 mK to 800 K

Cryocoolers

Dilution Refrigerator Systems

Micro-manipulated Probe Stations

LHe/LN₂ Cryostats

Magnet Systems

sales@janis.com www.janis.com

[Click to view our product web page.](#)

Momentum imaging spectrometer for molecular fragmentation dynamics induced by pulsed electron beam

EnLiang Wang, Xu Shan, YuFeng Shi, YaGuo Tang, and XiangJun Chen^{a)}

Hefei National Laboratory for Physical Sciences at Microscale and Department of Modern Physics, University of Science and Technology of China, Hefei, Anhui 230026, People's Republic of China

(Received 20 August 2013; accepted 28 November 2013; published online 18 December 2013)

A momentum imaging spectrometer has been built for studying the electron impact molecular fragmentation dynamics. The setup consists of a pulsed electron gun and a time of flight system as well as a two-dimensional time and position sensitive multi-hit detector. The charged fragments with kinetic energy up to 10 eV can be detected in 4π solid angles and their three-dimensional momentum vectors can be reconstructed. The apparatus is tested by electron impact ionization of Ar and dissociative ionization of CO₂. By analyzing the ion-ion coincidence spectra, the complete and incomplete Coulomb fragmentation channels for CO₂²⁺ and CO₂³⁺ are identified. The kinetic energy release (KER) and angular correlation for the two-body breakup channel CO₂^{2+*} → O⁺ + CO⁺ are reported. The peak value of total KER is found to be 6.8 eV which is consistent with the previous photoion-photoion coincidence studies, and the correlation angle of O⁺ and CO⁺ is also explicitly determined to be 172.5°.

© 2013 AIP Publishing LLC. [<http://dx.doi.org/10.1063/1.4847156>]

I. INTRODUCTION

The understanding of the fragmentation dynamics of multiply ionized molecules still remains a major challenge.^{1,2} Numerous studies have been devoted to the molecular fragmentation induced either by photons,^{3–5} electrons,^{6–8} as well as by heavy ions.^{9,10} Time of flight (TOF) spectrometer, in combination with multi-coincidence techniques, is usually employed to unveil the dissociation dynamics of various channels. The past decades have witnessed tremendous progress in momentum imaging techniques. With the development of the time and position sensitive multi-hit detector, all the charged products in a collision can be recorded event by event and the three-dimensional momentum vectors for all the fragment particles can be reconstructed. The Cold Target Recoil Ion Momentum Spectroscopy (COLTRIMS) or reaction microscopes has come up as a powerful tool in collision dynamics.^{11,12} The central issue in the molecular dissociation experiments is to improve the collection efficiency of the high energy fragments with favorable resolutions. In the previous studies,^{13–15} a short length of TOF system, a large area position sensitive detector (PSD), and a strong extraction field (typically several tens of V/cm) are adopted. Thanks to the advances in the momentum imaging techniques, in the past years, progresses have been made in investigations of fragmentation dynamics in diatomic molecules,¹⁶ polyatomic molecules,^{17,18} and interestingly in unveiling sequential and non-sequential Coulomb explosion (CE) processes.^{5,10}

Almost all the present available instruments for fragmentation studies adopt a transverse configuration where the incident beam is perpendicular to the axis of the TOF system. For the transverse spectrometer, it is easier in installation and commissioning, and there is no dead area in the detector. There is also longitudinal spectrometer, where the incident

particles fly along the axis of the TOF system, being used.¹³ However, the detector of this spectrometer must be specially designed. In fact, detector with a hole on it is adopted and the dead detection area is inevitable.

Though the superiority of the transverse spectrometer in investigating the fragmentation dynamics is obvious, it is difficult to carry out such experiment induced by electron impact. Because of the very light mass of electrons, they will be significantly deviated from the reaction center by the extraction field. Recently, Sharma and Bapat¹⁹ and Singh *et al.*²⁰ have reported their apparatuses for studying electron impact molecular fragmentation. In the work of Sharma and Bapat,¹⁹ a special electron optical lens is designed to compensate the deviation of the electron beam can be eliminated to some extent. However, the uniform extraction field is more or less disturbed. There is no special design of electron optical lens in the apparatus of Singh *et al.*²⁰ They just use very high energy electron beam (10 keV) to reduce the influence of the extraction field. However, the deviation of the electron beam cannot be virtually eliminated.

In this paper we report a momentum imaging spectrometer established in our laboratory for molecular fragmentation dynamics studies. Different from the previously reported apparatus,^{19,20} a pulsed electron beam is introduced to create single or multiple ionizations of target molecules. To eliminate the influence of the extraction field to the electron beam, a pulsed extraction field is introduced to work with the pulsed electron beam. When the electron pulse passes through the reaction center, the extraction voltage is powered off to keep the collision region field free. Just after the collision happens, the extraction voltage is powered on to create a uniform field to extract the charged fragments. There are several other advantages of using the pulsed electron beam. In actual experiment, we find that the background was significantly reduced. This might be because the ions can only be produced within the duration of the electron pulse (typically < 40 ns). Another

^{a)}xjun@ustc.edu.cn

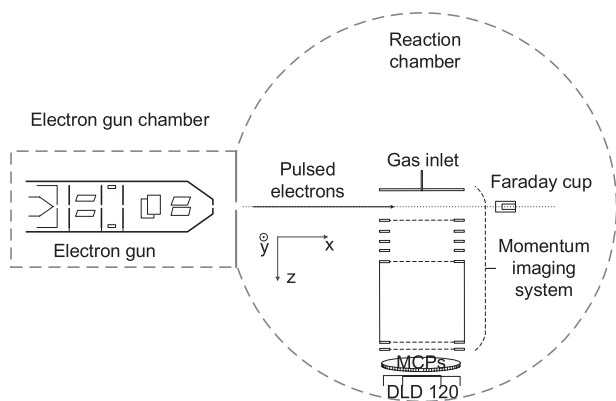


FIG. 1. Schematic of the experimental setup. The pulsed electron beam is perpendicular to the gas beam which coincides with the axis of momentum imaging system.

advantage of our design is the way to do the coincidence. In the instruments of Sharma and Bapat¹⁹ and Singh *et al.*,²⁰ the fragments are detected in coincidence with the ejected electrons in the opposite direction of ions. Due to the possible anisotropic distribution of the ejected electrons, the dynamics of the fragmentation may be affected. In our design, the trigger of the electron gun is used as the start signal for the coincidence measurement. As a result, all of the charged fragments of each collision will be extracted and detected in coincidence. The detector used in our setup has larger active area and the high energy fragment ions up to 10 eV can be detected in 4π solid angle. The apparatus has been tested by electron impact ionization of Ar and CO₂, and the dissociation of channel CO₂^{2+*} \rightarrow O⁺ + CO⁺ is analyzed in detail.

II. APPARATUS

The schematic of the experimental setup is shown in Fig. 1. A pulsed electron beam from a thermal cathode electron gun is injected into the reaction chamber to collide with the gas target at the reaction center. The pulsed electron gun and its power supply (EGG-3101/EGPS-3101) were purchased from Kimball Physics Company.²¹ The electron energy and pulse duration ranges are from 100 eV to 10 keV and 10 ns to 500 ns, respectively. The spot size of the electron beam at the reaction point is less than 1 mm when the electron gun is working under the recommended operating conditions. The electron beam is monitored by a Faraday cup which consists of a 6 mm diameter outer cup and 1 mm diameter inner cup. The typical beam current is kept less than 40 pA (effective value) to reduce the random coincidence. The target gas effuses from a capillary mounted on the pushing electrode of the momentum imaging system (MIS). The inner diameter and length of the capillary are 0.25 mm and 60 mm, respectively. The high ratio of length to inner diameter of the capillary enables a collimated gas beam. The target density at reaction point is about 10^{12} – 10^{13} /cm³. After collision between the electrons and target, a voltage pulse is applied on the pushing electrode to create a uniform field at the reaction area and to extract the fragment ions into the MIS which are then detected by the PSD comprised of a pair of micro-channel plates (MCPs) of 100 mm diameter in chevron

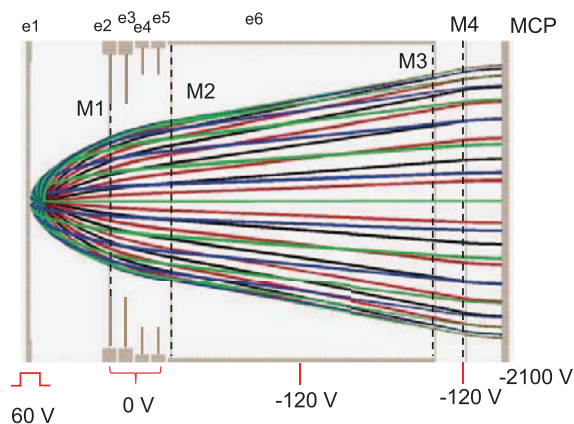


FIG. 2. Geometric diagram of momentum imaging system and simulation of 10 eV protons. The extraction field of acceleration region is 25 V/cm. The ion source is defined as spherical distribution with diameter of 2 mm. The emission angle step of protons is 10°.

configuration followed by delay line anode (DLD120) purchased from RoentDek.²² The vacuum system consists of a reaction chamber and an electron gun chamber. The reaction chamber is shielded by two layers of μ -metal. The residual magnetic field is less than 10 mG. Each chamber is pumped by a 700 l/s turbo-molecular pump. The background vacuum is better than 8×10^{-6} Pa.

A. Momentum imaging system

The kinetic energies of the molecular fragments usually range from several eV to several tens of eV. We design a three-dimensional focusing optics to improve the detection efficiency of the energetic ions. The schematic of the ion optics for the MIS is shown in Fig. 2. The fragment ions flying from reaction point to detector encounter three regions separated by two meshes (M1, M2). The voltages on electrodes e1 and e2 (M1) create a uniform electric field to push the fragment ions flying toward the detector. The ions are then focused between M1 and M2 by a non-uniform electric field created by e2–e6. As a result, the ions originated from different reaction point with identical momentum will hit the detector on the same point. The distance from reaction point to M2 is 40 mm. The electrode e6 is a field-free drift tube in which the ions will fly freely to the detector.

The plane electrode e1 is made of oxygen-free copper (100 mm \times 100 mm \times 2 mm). All of the remaining ones are made of non-magnetic stainless steel (316L). The first mesh, M1, of 64% transmission rate is mounted on e2 by silver conductive paint. The inner diameters of e3–e5 are 60 mm, 78 mm, and 78 mm, respectively. The outer and inner diameters of the drift tube (e6) are 100 mm and 96 mm and its length is 80 mm. Both sides of the drift tube are shielded by meshes, M2 and M3. The input surface of the MCPs is kept at high negative voltage to achieve a favorable detection efficiency of the ions. In order to prevent field penetration, another mesh M4 is installed between the drift tube and the MCPs to screen the high voltage potential of the surface of MCPs. The transmission rates of M2–M4 are 80%, 64%, and 64%, respectively. In actual experiment no influence to the

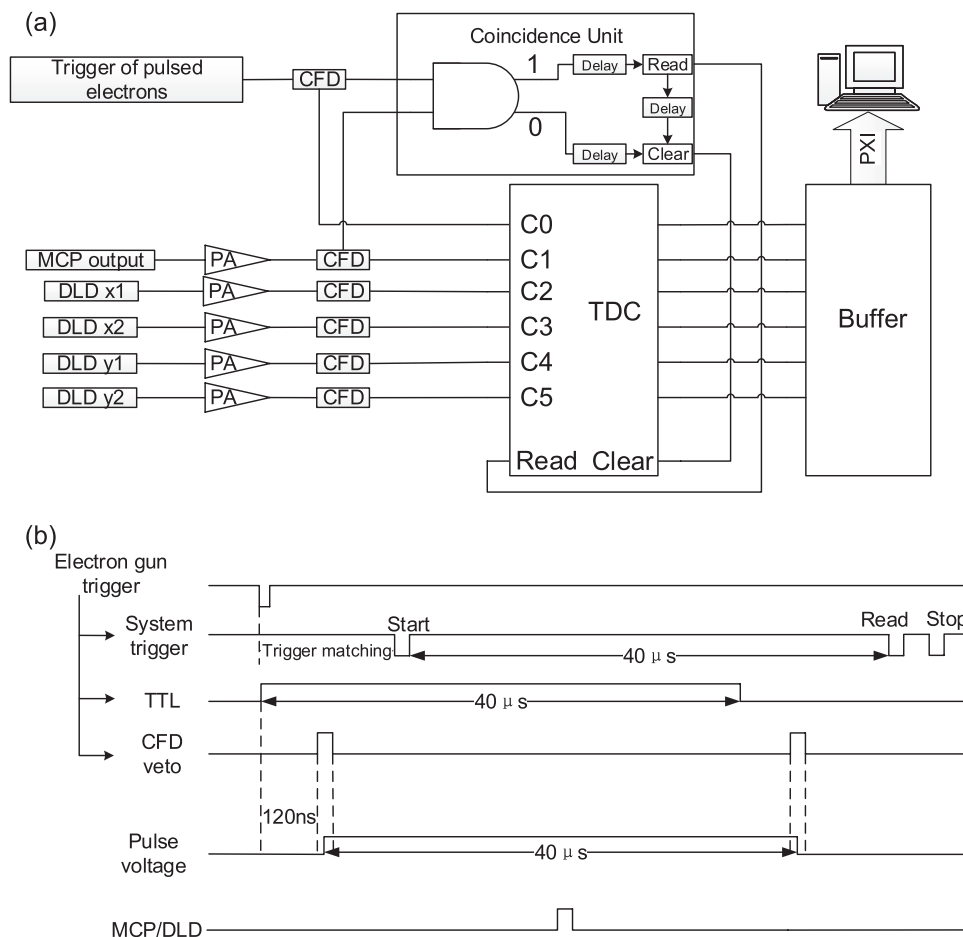


FIG. 3. Schematic of (a) data acquisition system and (b) timing diagram. DLD is delay line anode purchased from RoentDek. PA (preamplifier) is ORTEC VT120. CFD (constant fraction discriminator) is ORTEC 935. The coincidence unit and TDC (time to digital convert) are designed based on field programmable gate array chip (Xilinx Virtex 4).

electron beam is observed when the high voltage of MCPs is powered on.

After collision of the incident electron pulse with target molecules, a 40 μs duration pulsed voltage of 60 V whose rising time is less than 15 ns is applied to e1 to extract the charged fragments. The electrodes e2–e5 are held on ground voltage. The drift tube and M4 are both kept at −120 V. The electrodes e1 and e2 create a uniform electric field (25 V/cm throughout this work) in the extraction region. The voltage of front surface of the MCP pairs is kept at −2100 V, while the back surface is grounded.

The trajectories of 10 eV protons simulated by SIMION²³ program are also presented in Fig. 2. All of the ions can be extracted and projected onto the MCPs. By increasing the voltage on e1 higher energy ions can also be detected. In the simulation, the protons are ejected from a spherical source of 2 mm diameter. The emission angles are from 0° to 360° with step of 10°. As shown in Fig. 2, protons with same emission angle are well focused on the plane of MCPs.

B. Data acquisition system (DAQ)

The schematic of the DAQ is shown in Fig. 3(a), and the corresponding timing diagram is shown in Fig. 3(b). The trig-

ger of the pulsed electron gun is used as the time reference of the TOF of the ions. The coincidence unit accepts the trigger and the RC coupled timing signal from the exit plane of stack of MCPs to produce coincidence signal of a true event. The data stored in the time to digital converter (TDC) will be read into the buffer if the coincidence unit detects a true event, otherwise the data will be cleared after a fixed delay relative to the trigger.

As shown in Fig. 3(a), six signals are recorded in the TDC. The trigger of pulsed electron gun is recorded in TDC channel C0. The channel C1 records the MCP output signal. The position signals (DLD x1, x2, y1, and y2) are obtained by differentially amplifying the signals from the signal and reference wires of DLD120. All of the signals from the detector are first preamplified (PA) and then discriminated by the constant fraction discriminators (CFDs). The TOF is obtained by time difference of TDC channel C1 and C0. The position of the detected ion is encoded by the signal arrival time difference at both ends for each parallel pair delay-line, for each dimension independently,

$$x = c_x(t_{x1} - t_{x2}), \quad (1)$$

$$y = c_y(t_{y1} - t_{y2}), \quad (2)$$

where t_{xi} , t_{yi} ($i = 1, 2$) are time signals from delay-lines recorded in TDC and c_x , c_y are calibration coefficients.

Figure 3(b) shows the timing diagram. The trigger signal of the pulsed electron gun is divided into three. The first one is used to produce the system trigger of the coincidence unit. After a delay of typical 40 μ s, the data will be read or cleared by stop signal depending on the output of the coincidence unit. The second one is converted into TTL (Transistor-Transistor Logic) signal to control the pulse voltage power supply. At the leading and trailing edge of the pulse voltage a lot of noise will be coupled into the detector which will cause false events in data acquisition. We design a circuit to produce a CFD veto signal, which is triggered by the third copy of the trigger signal, to disable the CFDs during the state transition of the pulse voltage to avoid the noise. In the present experimental conditions, the TOF of the fastest ion, proton, is about 1100 ns, while the time interval between the electron and extraction pulses is about 120 ns and the width of CFD veto signal is 500 ns. So the fastest ions will not be lost. In the actual DAQ system, the time interval between the electron and extraction pulses can further be reduced to less than 25 ns by applying a delay to the trigger signal.

The coincidence unit and the TDC are developed in one Field Programmable Gate Array (FPGA) chip (Xilinx Virtex-4). The working principle of the multi hit TDC has been well described elsewhere.²⁴ Briefly, the 120 MHz reference clock produces 8.333 ns resolution coarse time and the 176 element delay cells give out 47 ps per bin size. The standard deviation of time measurement is less than 30 ps before correction and typically about 21 ps after correction. The data of true events are stored in list format file in computer.

The data analysis program is developed based on Go4²⁵ package. The physical information of the molecular fragments are reconstructed by the TOF and hit positions of the ions.²⁶ The relationship between the momentum and TOF or hit positions are described by

$$p_x = m \frac{x}{TOF}, \quad (3)$$

$$p_y = m \frac{y}{TOF}, \quad (4)$$

$$p_z = QE(T_0 - TOF), \quad (5)$$

where p_i ($i = x, y, z$) and m are the momentum components and mass of the detected ion. Q and E are the charge state of the ion and the magnitude of the extraction field. T_0 is the central value of TOF corresponding to the ions which have zero initial kinetic energy.

III. CALIBRATIONS OF SPECTROMETER

A. Calibration of PSD

The PSD is calibrated by 2.5 keV electron impact ionization of H_2 . The H_2 is chosen because of the significant distribution of high energy protons from the fragmentations and, as a result, all the active areas of PSD can be hit on. In the calibration, a mask is mounted in front of the MCPs. As shown in Fig. 4(a), the mask is made of a copper plate with

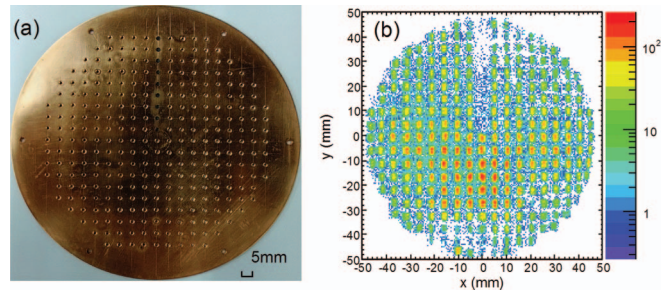


FIG. 4. (a) Calibration mask and (b) the relevant position image of mask.

arrays of holes on it. The diameter of each hole is 1.0 mm and the distance between two neighboring holes is 5.0 mm. The positions of the holes of the mask are accurately determined in machining and used as the calibration standard for the PSD. Nine holes on the central top of the mask are blocked by graphite as a referential direction. The position image of protons is shown in Fig. 4(b). To evaluate the linearity and resolution of the PSD we project the data of Fig. 4(b) to x axis and y axis, respectively. The data after projection are shown in Figs. 5(a) and 5(b). Each peak in Figs. 5(a) and 5(b) is fitted using a Gaussian function, and the fitted peak positions are considered as the observed positions of the holes. The full width at half maximum (FWHM) of the fitted peak is the convolution of the diameter of the hole (1.0 mm) and the resolution of the PSD. After deconvolution of the intrinsic width of the mask, the resolution of the PSD is determined to be better than 0.5 mm. The observed positions are plotted against the physical positions of the holes for both x and y dimensions as shown in Figs. 5(c) and 5(d). The linear fits to the measured, shown in the same figure, indicate the good linear response of the PSD.

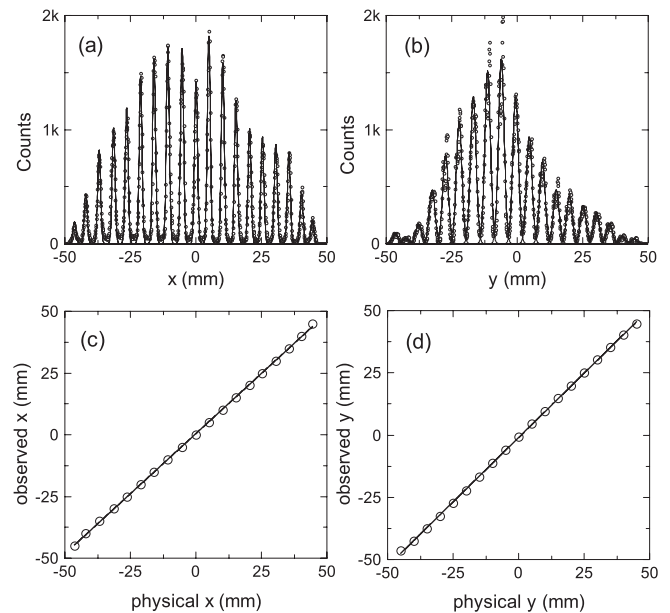


FIG. 5. Projection distributions of the images of mask and linearity of the PSD. (a) x direction distribution. (b) y direction distribution. (c) The observed positions against the physical positions in x direction. (d) The observed positions against the physical positions in y direction.

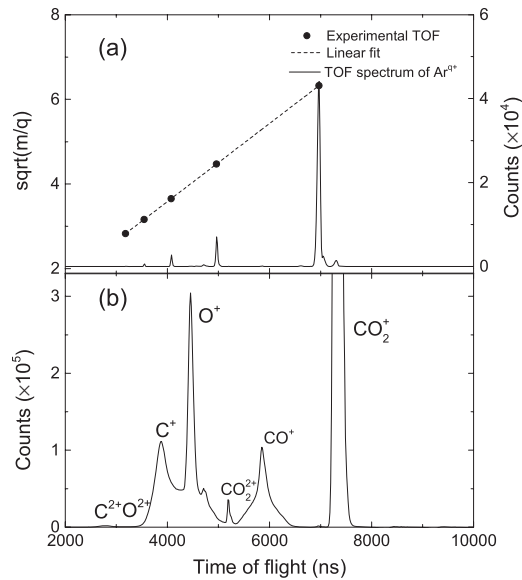


FIG. 6. (a) TOF spectrum of Ar^{q+} and relevant calibration curve. (b) TOF spectrum of ionic fragments arising from electron impact ionization of CO_2 . The extraction field of both samples is 25 V/cm. The TOF is obtained by the time difference between the first hit ions and the trigger of pulsed electron gun.

B. Calibration of TOF

The TOF system is calibrated by 5.0 keV electron (pulse width is 35 ns with repetition frequency of 10 kHz) impact single and multiple ionizations of Ar atom. The count rate of the ion detector which depends on the pulse width and the repetition frequency of the electron beam is less than 300 s^{-1} at present experimental conditions. The event rate is far less than the repetition of the electron beam which ensures that there is less than one target atom ionized in one pulse. For different charge states of Ar ions, TOFs are proportional to the square root of the mass to charge ratios $[(m/q)^{1/2}]$, where m and q are mass and charge state of Ar ions, respectively. The positions of TOF peaks for different charged ^{40}Ar is plotted as a function of $(m/q)^{1/2}$ in Fig. 6(a). The linear fitting agrees well with the experiments indicating a good linearity of the TOF system. The width of the Ar^+ peak may essentially be taken as the limit of mass resolution. The FWHM of the Ar^+ peak is 66.6 ns, while the TOF of Ar^+ is 6950.5 ns. This gives a mass resolution $m/\Delta m = 104$. The calculated mass resolution is about 124 for the effusive gas beam at room temperature based on Wiley-McLaren equations,²⁷ which is consistent with experiment. The resolution is sufficient to resolve the fragments from the small molecules.

C. Calibration of MIS

We choose CO_2 as the sample to test the performance of MIS since it has been studied^{5,8–10,19,20,28} in detail. The experiment has been carried out at an impact energy of 5.0 keV (electron pulse width is 35 ns with repetition frequency of 10 kHz). The TOF of the first hit ions is shown in Fig. 6(b). The most intense and sharp peak originates from the single ioniza-

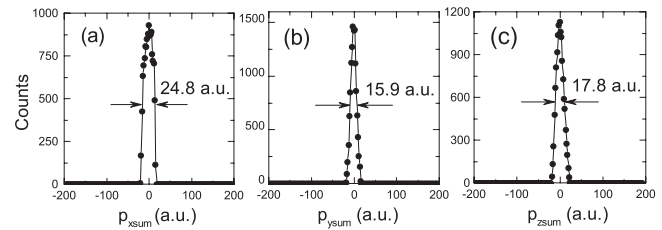


FIG. 7. Momentum resolution of (a) x direction of electron beam, (b) y direction, and (c) z direction which is TOF axis.

tion of CO_2 . Other peaks can be assigned to CO_2^{2+} which is due to the direct double ionization, as well as CO^+ , O^+ , C^+ , O^{2+} , and C^{2+} originated from the dissociative ionizations.

The momentum resolution is determined employing the same method as in Ref. 20. For the complete Coulomb fragmentation process $\text{CO}_2^{2+*} \rightarrow \text{O}^+ + \text{CO}^+$, the momenta of the two fragments comply with the conservation of momentum, $\vec{p}_1 + \vec{p}_2 = 0$. The experimental value of $\vec{p}_1 + \vec{p}_2$ thus has a distribution around zero, the width of which reflects the momentum resolution of the MIS. The distributions of the summations of the three momentum components are presented in Fig. 7. The observed momentum resolutions for these components are determined to be 24.8 a.u., 15.9 a.u., and 17.8 a.u., respectively. The observed momentum resolution is a combined contribution from the instrumental resolution and thermal distribution of the targets. Therefore, the momentum resolution can be further optimized by reducing the size of the collision point and the temperature of the target gas, e.g., employing a cold supersonic gas beam.

IV. RESULTS AND DISCUSSION

A. Ion-ion coincidence

The ion-ion coincidence can be achieved by drawing two-dimensional spectrum of the TOF of the fragment ions. The true events are scattered along diagonal lines resulting from the correlation in the TOF between the two fragments from the dissociative ionization of molecule. This two-dimensional spectrum is usually referred to as coincidence map which has been widely used in fragmentation studies^{29–31} and proved to be a powerful tool in identifying the dissociation channels. For a certain channel, the true events will distribute along an island on the coincidence map, the slope of which reflects the momentum correlation of the fragments. Analyzing from Eq. (5), the slope of the island can be approximated by

$$k = \frac{p_{2z}}{Q_2} \frac{Q_1}{p_{1z}}, \quad (6)$$

where p_{iz} and Q_i ($i = 1, 2$) are the z component of momentum and charge state of the ions.

The coincidence maps for electron impact ionization dissociation of CO_2 are shown in Fig. 8. Figure 8(a) represents the correlation of the first and second ions. Three islands (a1, a2, and a3) corresponding to the coincident ion pairs of $\text{O}^+ + \text{CO}^+$, $\text{O}^+ + \text{O}^+$, and $\text{C}^+ + \text{O}^+$ are observed in Fig. 8(a), which can be ascribed to the following dissociative channels

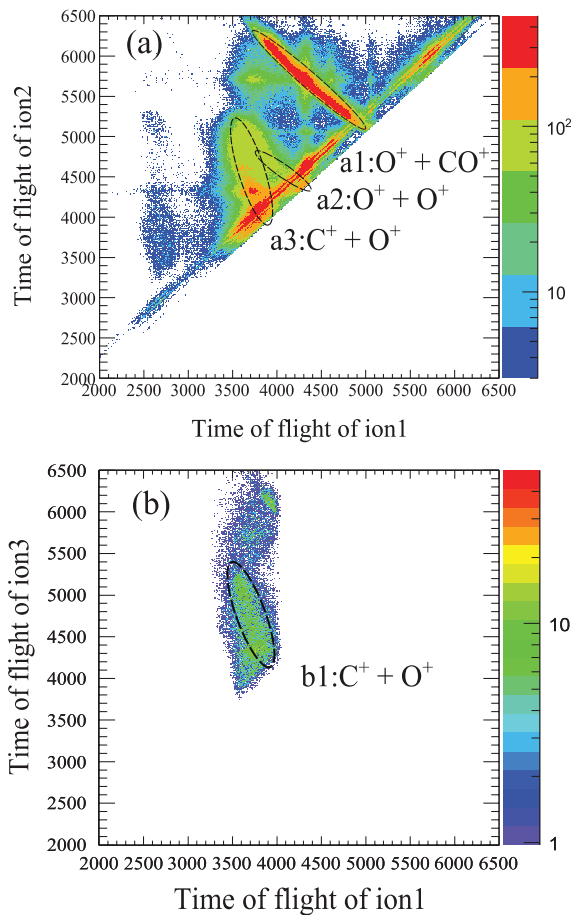
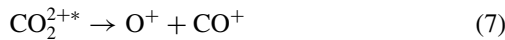
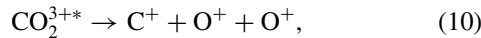


FIG. 8. Ion-ion coincidence spectrum of the fragments of CO₂. (a) The first versus the second ions. (b) The first versus the third ions after choosing island a3.

of CO₂^{2+*}:



The first coincident pair is due to the two-body breakup channel (7). The second and third pairs are arisen from the three-body fragmentation in channels (8) and (9), with third partner being neutral C and O, respectively. The third coincident ion pairs of C⁺ + O⁺ may also originate from the complete Coulomb fragmentation of CO₂^{3+*},



where the third partner is another O⁺. For this channel, a third ion (O⁺) will be detected in sequence by the multi-hit detector. In order to get information on this triple coincidence, the coincidence map of the first (C⁺) and the third (O⁺) ions is drawn in Fig. 8(b) after choosing island a3. A coincidence island (b1) of C⁺ and O⁺ is observed. By choosing island a3, the first (C⁺) and second (O⁺) ions are detected in coincidence, while b1 correlates the first (C⁺) and the third (O⁺) ions. In this way, triple coincident measurement on channel (10) can be achieved.

The strong and broad signals along the diagonal T1 = T2 in Fig. 8(a) are caused by the mis-trigger of the same single

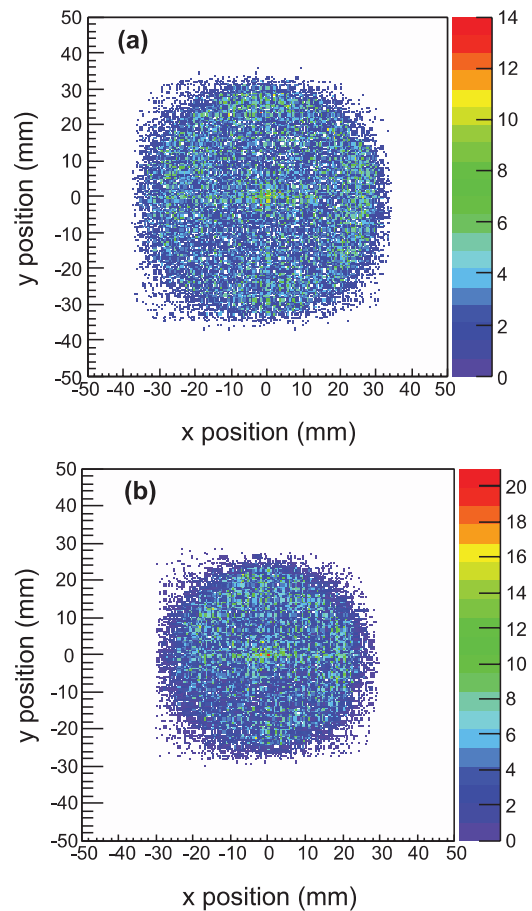


FIG. 9. Position distributions of (a) O⁺ and (b) CO⁺.

time signal of the first hit ion due to its oscillating tail. Fortunately, these signals can be filtered by further analyzing the momentum correlation in x or y dimensions. If we draw the correlation map of p_x or p_y between ion pairs, the true events will also locate along diagonal lines due to momentum correlation of the fragments.

B. Kinetic energy release distribution

Two-dimensional position distributions (PD) of O⁺ and CO⁺ from channel (7) are shown in Figs. 9(a) and 9(b). Due to the proportional relationship between position (x, y) and momentum (p_x, p_y), these spectra essentially correspond to p_x - p_y distributions. It can be seen clearly that the overall features of the PD are quite homogenous indicating an isotropic fragmentation. Besides, the size of the image of O⁺ is larger than that of CO⁺, which indicates that O⁺ carries more kinetic energy than CO⁺ after Coulomb fragmentation.

The total kinetic energy release (KER) distribution as well as KER distributions for the two associated fragments of channel (7) have been obtained and shown in Fig. 10. The total KER ranges from 0 eV to 14 eV with peak value at 6.8 eV. The peak values of KER of O⁺ and CO⁺ are 4.2 eV and 2.35 eV, respectively. Due to the conservation of momentum, the kinetic energy of the light mass ion (O⁺) is larger than that of the large mass one (CO⁺). The ratio of the peak values of KER of O⁺ and CO⁺ is 1.79 which agrees well

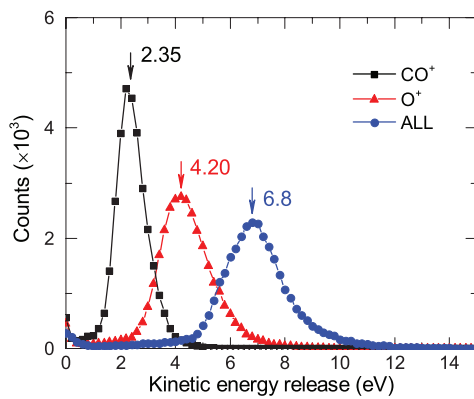


FIG. 10. Kinetic energy release distribution of complete Coulomb fragmentation of CO_2^{2+*} induced by 5.0 keV electron.

with the mass ratio of CO^+ to O^+ (1.75). Our result of total KER (6.8 eV) is in line with the photoion-photoion coincidence (PIPICO) studies by Dujardin and Winkoun.³² In their work, they concluded that there exist three distinct channels for the dissociation of CO_2^{2+*} into $\text{CO}^+ + \text{O}^+$ corresponding to a mean KER of, respectively, 4.5 eV, 6.5 eV, and 9.4 eV. In the present electron impact experiment with incident energy of 5.0 keV, all of the three channels are open. This leads to an average value of KERs to be measured which is precisely 6.8 eV. Lower values of KERs were estimated by Sharma and Bapat¹⁹ (5.9 eV) and Bhatt *et al.*⁸ (4.7 eV). This may be due to their incomplete collection of the high energy ions as had been discussed in Ref. 20.

C. Angular correlation

The correlation angle (γ) of two fragments can be deduced from their momentum vector (\vec{p}_1, \vec{p}_2):

$$\gamma = \cos^{-1} \left(\frac{\vec{p}_1 \cdot \vec{p}_2}{|\vec{p}_1||\vec{p}_2|} \right). \quad (11)$$

For the complete Coulomb fragmentation process $\text{CO}_2^{2+*} \rightarrow \text{O}^+ + \text{CO}^+$, the experimental distribution of the correlation angle γ between two fragments O^+ and CO^+ can be obtained from Eq. (11) and the result is shown in Fig. 11. The most probable value can be explicitly determined to be 172.5° , which is consistent with the previous studies.^{8,28} The experimental result reveals that in this two-body dissociation process, instead of leaving exactly 180° apart, CO^+ ions emit around 172.5° respective to the momentum vector of O^+ . This may possibly be due to the vibrational and rotational motions during the dissociation.

V. SUMMARY

A momentum imaging spectrometer has been built to investigate molecular fragmentation dynamics. Three-dimensional momentum vectors of all the charged fragments can be reconstructed. The performance of the setup has been tested by 5.0 keV electron impact ionization of Ar and dissociative ionization of CO_2 . The KER distributions and angular correlation of the complete Coulomb fragmentation channel

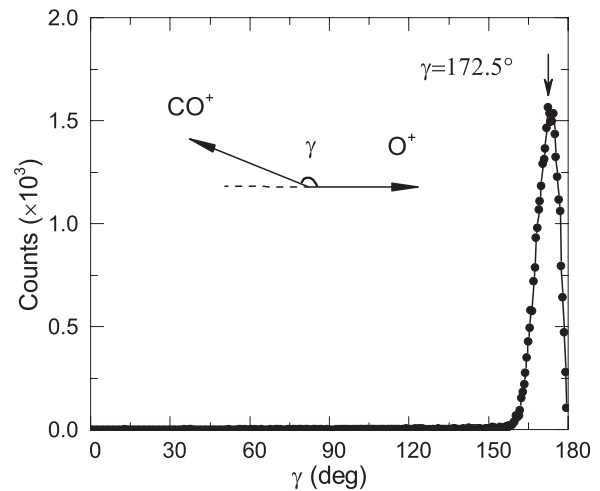


FIG. 11. Correlation angle distribution of two fragments of channel $\text{CO}_2^{2+*} \rightarrow \text{O}^+ + \text{CO}^+$.

$\text{CO}_2^{2+*} \rightarrow \text{O}^+ + \text{CO}^+$ have been obtained. It is found that the peak values of KER distributions for O^+ , CO^+ , and their total are 4.2 eV, 2.35 eV, and 6.8 eV, respectively. The total KER is consistent with the previous PIPICO studies. The correlation angle of O^+ and CO^+ is also explicitly determined to be 172.5° . In the future, two spherical analyzers for detecting scattered and ejected electrons will be mounted in the system. The excitation dissociation or ionization dissociation dynamics can be carried out with high energy resolution (e, e-ion) or (e, 2e-ion) experiments.

ACKNOWLEDGMENTS

This work was jointly supported by the National Basic Research Program of China (Grant No. 2010CB923301), the National Natural Science Foundation of China (Grant Nos. 10979007 and 10734040), the CAS knowledge promotion project (No. KJCX1-YW-N30), and the Fundamental Research Funds for the Central Universities.

- ¹D. Mathur, *Phys. Rep.* **225**, 193 (1993).
- ²K. Ueda and J. H. D. Eland, *J. Phys. B* **38**, S839 (2005).
- ³J. H. D. Eland, *Mol. Phys.* **61**, 725 (1987).
- ⁴M. Lavollée and H. Bergeron, *J. Phys. B* **25**, 3101 (1992).
- ⁵C. Wu, C. Wu, D. Song, H. Su, Y. Yang, Z. Wu, X. Liu, H. Liu, M. Li, Y. Deng, Y. Liu, L. Peng, H. Jiang, and Q. Gong, *Phys. Rev. Lett.* **110**, 103601 (2013).
- ⁶T. Kerkau, B. Krässig, O. Schwarzkopf, H. Kossmann, B. Kämmerling, and V. Schmidt, *Nucl. Instrum. Methods Phys. Res. A* **479**, 555 (2002).
- ⁷G. Alberti, E. Fainelli, F. Maracci, M. Mastropietro, R. Platania, and L. Avaldi, *Rev. Sci. Instrum.* **76**, 073101 (2005).
- ⁸P. Bhatt, R. Singh, N. Yadav, and R. Shanker, *Phys. Rev. A* **85**, 042707 (2012).
- ⁹B. Siegmund, U. Werner, H. O. Lutz, and R. Mann, *J. Phys. B* **35**, 3755 (2002).
- ¹⁰N. Neumann, D. Hant, L. Ph. H. Schmidt, J. Titze, T. Jahnke, A. Czausch, M. S. Schöffler, K. Kreidi, O. Jagutzki, H. Schmidt-Böcking, and R. Dörner, *Phys. Rev. Lett.* **104**, 103201 (2010).
- ¹¹R. Dörner, V. Mergel, O. Jagutzki, L. Spielberger, J. Ullrich, R. Moshhammer, and H. Schmidt-Böcking, *Phys. Rep.* **330**, 95 (2000).
- ¹²J. Ullrich, R. Moshhammer, A. Dorn, R. Dörner, L. Ph. H. Schmidt, and H. Schmidt-Böcking, *Rep. Prog. Phys.* **66**, 1463 (2003).
- ¹³A. Senftleben, O. Al-Hagan, T. Pflüger, X. Ren, D. Madison, A. Dorn, and J. Ullrich, *J. Chem. Phys.* **133**, 044302 (2010).

- ¹⁴S. Bellm, J. Lower, D. Mueller, and E. Weigold, *J. Phys.: Conf. Ser.* **212**, 012005 (2010).
- ¹⁵D. Nandi, V. S. Prabhudesai, E. Krishnakumar, and A. Chatterjee, *Rev. Sci. Instrum.* **76**, 053107 (2005).
- ¹⁶R. Singh, P. Bhatt, N. Yadav, and R. Shanker, *Phys. Rev. A* **87**, 022709 (2013).
- ¹⁷R. Singh, P. Bhatt, N. Yadav, and R. Shanker, *J. Phys. B* **46**, 085203 (2013).
- ¹⁸P. Bhatt, R. Singh, N. Yadav, and R. Shanker, *Phys. Rev. A* **86**, 052708 (2012).
- ¹⁹V. Sharma and B. Bapat, *Eur. Phys. J. D* **37**, 223 (2006).
- ²⁰R. Singh, P. Bhatt, N. Yadav, and R. Shanker, *Meas. Sci. Technol.* **22**, 055901 (2011).
- ²¹See www.kimballphysics.com for key characteristics of the electron gun systems (model EGG-3101).
- ²²See www.roentdek.com for details and manuals of the delay line anode.
- ²³See www.simion.com for introductions and supports of SIMION program.
- ²⁴J. Wang, S. Liu, L. Zhao, X. Hu, and Q. An, *IEEE Trans. Nucl. Sci.* **58**, 2011 (2011).
- ²⁵See www-win.gsi.de/go4/ for downloading the source code and manuals of Go4 package.
- ²⁶J. Ullrich and V. P. Shevelko, *Many-Particle Quantum Dynamics in Atomic and Molecular Fragmentation* (Springer, Berlin, 2003).
- ²⁷W. C. Wiley and I. H. McLaren, *Rev. Sci. Instrum.* **26**, 1150 (1955).
- ²⁸B. Bapat and V. Sharma, *J. Phys. B* **40**, 13 (2007).
- ²⁹L. J. Frasinski, K. Codling, and P. A. Hatherly, *Science* **246**, 1029 (1989).
- ³⁰P. Wang and C. R. Vidal, *J. Chem. Phys.* **118**, 5383 (2003).
- ³¹R. Singh, P. Bhatt, N. Yadav, and R. Shanker, *Phys. Rev. A* **87**, 062706 (2013).
- ³²G. Dujardin and D. Winkoun, *J. Chem. Phys.* **83**, 6222 (1985).